Performance of a cerium fluoride crystal matrix measured in high-energy particle beams

E. Auffray, T. Beckers, J. Bourotte, R. Chipaux, V. Commichau, I. Dafinei, P. Depasse, L. Djambazov, U. Dydak, H. El Mamouni, et al.

EUROPEAN ORGANIZATION FOR NUCLEAR RESEARCH

CERN–PPE/95–176
October 23, 1995

PERFORMANCE OF A CERIUM FLUORIDE CRYSTAL MATRIX MEASURED IN HIGH-ENERGY PARTICLE BEAMS

E. Auffray[1], T. Beckers[2], J. Bourrotte[3], R. Chipaux[4], V. Commichau[5], I. Dafinei[1], P. Depasse[6], L. Djambazov[7], U. Dydak[1], H.El Mamouni[6], J. Fay[6], M. Felcini[7], M. Goyot[6], M. Haguenauer[3], K. Hangarter[5], H. Hillemanns[8], H. Hofer[7], B. Ille[6], B. Jacobs[9], T. Kirn[8], D. Kryn[6], P. Lebrun[6], P. Lecomte[7], P. Lecoq[1], J.P. Martin[6], M. Mattioli[10], G. Maurelli[6], I. Melnikov[7], F. Nessi-Tedaldi[7], L. Pacciani[10], S. Pirro[10], R. Raghavan[11], D. Ren[7], M. Reynaud[6], U. Röser[7], P. Sahuc[6], D. Schmitz[8], M. Schneegans[12], J. Schwenke[8], I. Soric[13], G. Viertel[7], H.P. Von Gunten[7], J.P. Walder[6], S. Waldmeier-Wicki[7].

Abstract:

A cerium fluoride matrix composed of nine longitudinally segmented towers, approximately 25 X_0 long, has been tested in electron, muon and pion beams of momenta ranging from 10 to 150 GeV/*c*. The results are discussed in terms of light yield, electronic noise, energy and position resolution. In spite of serious imperfections in geometry and quality of some of the crystals, an electron energy resolution of ~ 0.5% has been obtained with a silicon photodiode readout, for energies above 50 GeV. The performance of cerium fluoride in a beam, its high density, high light yield and fast response, radiation resistance and ruggedness make it a very good candidate for high-resolution calorimetry at future colliders. The optimisation of the production of large high-quality crystals is being studied in several firms over the world. Many CeF_3 crystals, 2×2 cm^2 or 3×3 cm^2 in cross-section and up to 28 cm long, were received in 1994 from four companies, some of them with excellent light yield and radiation hardness.

Submitted to Nuclear Instrument and Methods

---

1) CERN, Geneva, Switzerland.
2) UIA, Universitaire Instelling Antwerpen, Belgium.
3) Ecole Polytechnique, Palaiseau, France.
4) CEA, DSM / DAPNIA, Saclay, France.
5) IIIrd Physics Institute, RWTH Aachen, Germany.
6) IPNL, IN$_2$P$_3$-CNRS et Université Claude Bernard, Villeurbanne, France.
7) ETH, Swiss Federal Institute of Technology, Zürich, Switzerland.
8) Ist Physics Institute, RWTH Aachen, Germany.
9) VUB, Vrije Universiteit Brussels, Belgium.
10) INFN Roma, Italy.
11) TIFR, Tata Institute of Fundamental Research, Bombay, India.
12) LAPP, IN$_2$P$_3$-CNRS, Annecy-le-Vieux, France.
13) FESB, University of Split, Croatia.

1. INTRODUCTION

It is a well established fact [1], that high-resolution electromagnetic calorimetry is mandatory for physics at the Large Hadron Collider (LHC). Only homogeneous and 'dedicated' calorimeters may reach the ultimate resolution, needed in particular for Standard or Supersymmetric Higgs searches. Crystal calorimetry is presently the best and most reliable homogeneous technique [2], provided heavy, fast, radiation hard and relatively cheap scintillators can be produced.

The 'Crystal Clear' Collaboration (RD18) has conducted generic crystal research since 1990 [3]. The Swiss Federal Institute of Technology has since 1991 a joint research agreement with the Shanghai Institute of Ceramics and with the Beijing Glass Research Institute to produce and test large CeF_3 crystals. Both groups started end of 1993 a collaboration to evaluate the feasibility of a cerium fluoride calorimeter for the CMS experiment. The understanding of CeF_3 properties [4,5,6] and the capacity of industry for growing large crystals had sufficiently progressed to allow the CMS collaboration to consider a calorimeter based on this crystal for an experiment at LHC [7]. Several CeF_3 crystals were tested in 1993 in a beam by the RD18 collaboration [8]. The results presented here are based on data taken on a CeF_3 crystal matrix between April and September 1994 in two CERN/SPS test beams at momenta ranging from 10 to 150 GeV/*c*.

2. THE TEST SET-UP

2.1. The X_3 and H_4 beam lines

Most of our studies were performed in the X3 beam line of the SPS West area. It is a low intensity unseparated tertiary beam providing muons, pions and electrons of energies ranging from 4 to 50 GeV. The beam optics gives a ±0.5% electron momentum resolution for small collimator settings. This was confirmed by a measurement with the X3 beam spectrometer consisting of four delay wire chambers and two bending magnets [9]. The beam momentum spread was quadratically subtracted from the observed energy resolutions. Four scintillation counters allowed to define a wide beam of 1 cm^2 or a narrow beam of 0.4×0.4 cm^2. In the last condition, electron rates were of 10–50 particles in a 1.2 s burst occuring every 14 s. The crystal matrix could be displaced on a X,Y scanning table, about 1 m away from the trigger counters, with an accuracy better than 100 μm.

Electron data at higher energy were also taken over two days in the H4-beamline of the SPS North area with beam momentum resolutions varying from ±0.1% at 20 GeV to 0.25% at 150 GeV. Some magnet settings were extremely critical, so that variable pion contamination in the electron sample have to be taken into account. Scintillation counters defined a wide beam of 2×2 cm^2 or a narrow beam of 0.5×0.5 cm^2. Here again a scanning table enabled us to position each tower in the beam.

2.2. The CeF_3 matrix

The matrix, composed of nine longitudinally segmented towers of ~25 X_0 length, can be seen in Fig. 1. The segmentation was chosen to allow the reconstruction of the incoming particle direction by determining two independent barycentres (see Section 8). Parallelopipedic crystals, ~14 cm long, were produced by 4 firms: OPTOVAC (US), BGRI, SIC (China), and MKT (Czech Republic). The towers were made of a front segment, read by a Silicon PhotoDiode (SiPD) glued onto the front face, and of a back segment made of two crystals glued

together with a UV transparent glue [10] and viewed by a SiPD at the rear. The towers were 3×3 cm^2 in section, except for the 4 corners being 2×2 cm^2. Small variations in length and in section from crystal to crystal (see Table 1) created gaps and imperfections in alignment. The light yield also varied significantly from 280 to 1080 photons/MeV, as measured with a ^{137}Cs source and a XP 2020Q photomultiplier. The crystals were wrapped in Millipore [11], corrected when necessary by black scotch strips to uniformize the light collection efficiency.

Table 1

Dimensions, light yield and residual non-uniformity of the crystals. Light yield is the number of collected photons/MeV impinging on the PM, measured in the laboratory with a ^{137}Cs source. Non-uniformity is the relative difference between ends of a crystal with final wrapping. Tower 5 is in the centre.

Tower	Segment	Dimensions (mm)	Total tower length (mm)	Light Yield (photons/MeV)	Non-Uniformity (%)
1	Front	$20 \times 20 \times 126$		1082	4.2
	Back	$20 \times 20 \times (140+140)$	406	490	4.9
2	Front	$32 \times 33 \times 114$		1040	2.5
	Back	$30 \times 30 \times (140+140)$	394	380	12.2
3	Front	$20 \times 20 \times 140$		980	6.2
	Back	$20 \times 20 \times (100+167)$	407	1013	4.6
4	Front	$28 \times 29 \times 141$		720	6.4
	Back	$30 \times 30 \times (80+80+100)$	400	280	23.6
5	Front	$30 \times 30 \times 148$		550	8.3
	Back	$30 \times 30 \times (140+140)$	428	650	6.6
6	Front	$31 \times 31 \times 132$		370	11.3
	Back	$30 \times 30 \times (140+140)$	413	440	15.5
7	Front	$21 \times 21 \times 140$		846	9.7
	Back	$20 \times 20 \times (125+128)$	393	459	-4.3
8	Front	$28 \times 28 \times 141$		700	9.7
	Back	$29 \times 29 \times 255$	396	400	6.6
9	Front	$20 \times 20 \times 140$		523	8.8
	Back	$20 \times 20 \times (140+106)$	386	359	6.9

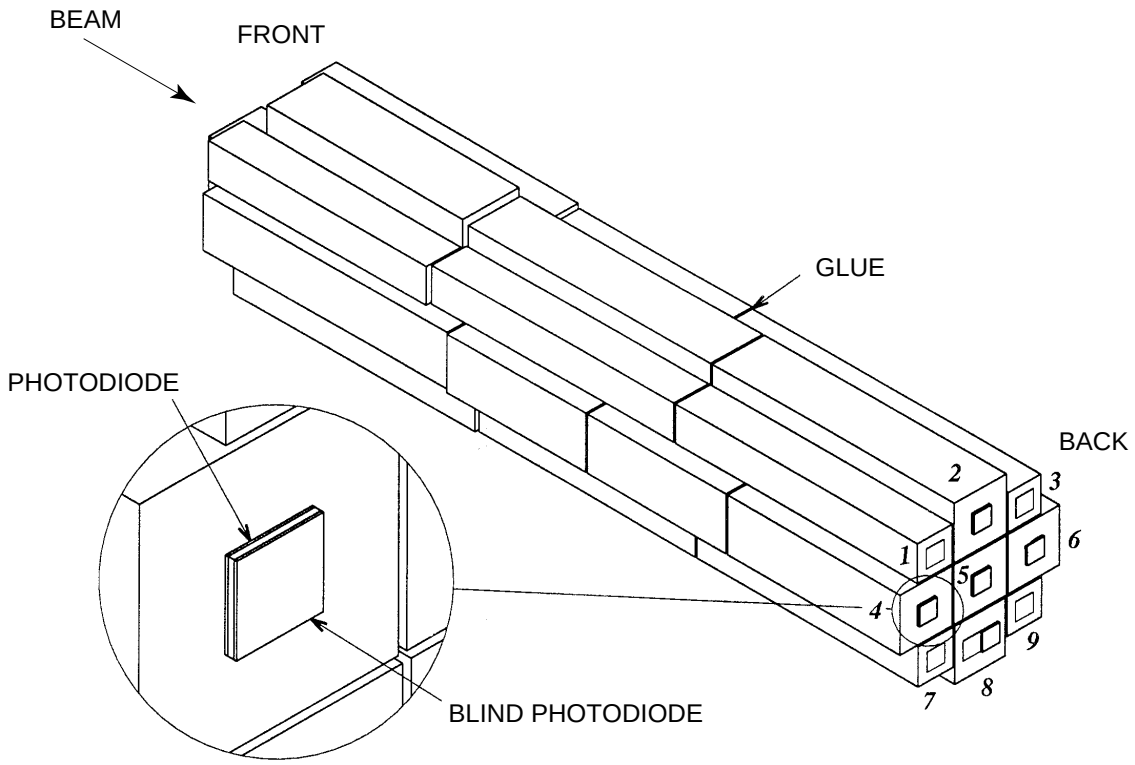

Fig. 1: The CeF_3 9-tower matrix geometry. The positioning of a 'blind' SiPD with respect to a SiPD seeing the crystal light is shown.

The SiPD were 1 cm^2 windowless PIN photodiodes, 300 μm thick (Hamamatsu 3590–04), with a quantum efficiency of 35–40% in the UV. They were optically coupled to the crystals by a viscous UV transparent glue [12]. Some lower light yield crystals were seen by 2 SiPD connected in parallel. The wrapped crystals were pressed together and placed inside a double shielded aluminum container. Short cables (~15 cm) linked the SiPDs to the preamplifier boards placed close to the front and back crystals. Three meter long cables connected the boards via a patch panel to the amplifiers. The small temperature dependence of the CeF_3 response (0.14%/^oC) made precise temperature regulation unnecessary.

Most of the results presented here were obtained with 2 μs signal shaping. Several types of fast amplifiers with a 20–30 ns peaking time were also evaluated in view of the preparation for the LHC requirements (see section 6).

In the first case, the electronic readout chain (Fig. 2) associated with each SiPD consisted of a charge preamplifier [13] and of a standard RC–CR shaping amplifier [14] with a time constant near to 2 μs. The shapers gave a positive output signal with remotely adjustable gain between 1 and 1600 and a fast negative signal for self-triggering purposes, used when calibrating each chain with gamma sources or cosmic rays.

The analog signals were digitised in CAMAC peak sensing ADCs [15], located ~60m away in the counting room. In the X3 area, the data acquisition was performed with a PC-based system, the data being transferred via ETHERNET at the end of each run to a UNIX computer for further analysis. In the H4 area, the data were acquired by a Lynx OS VME system and monitored on a UNIX workstation.

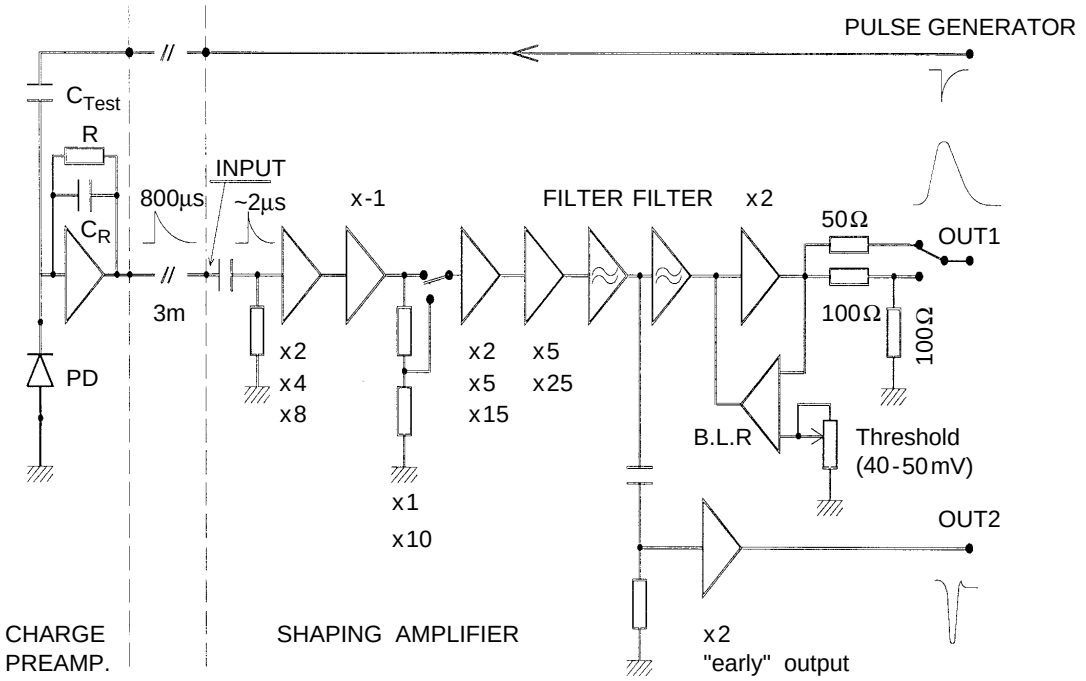

Fig. 2: Schematics of the electronic readout chain. B.L.R. means base line restorer.

3. ELECTRONIC CALIBRATION AND NOISE

The calibration, linearity and noise determination of the electronic chains have been performed with an ORTEC pulse generator and a ^{57}Co source. Calibration runs have been taken before and after each beam period. Mainly due to the baseline restorer of the shapers, the shaper-ADC chain exhibited small non-linearities at the low end of the dynamic range, which were corrected for.

The electronic noise of each channel, measured from ^{57}Co γ-source spectra (122 and 136 keV peaks) and pulse generator distributions, was found to be typically 730 and 840 e^- for respectively one and two photodiodes (~50 and ~100 pF capacitance). The fraction of correlated noise, determined from the ratio $\sigma(\Sigma_{9x2})/\sqrt{\Sigma_{9x2}\ \sigma_i^2}$, is about 20% for the whole matrix (18 channels).

Using the above calibrations, a noise equivalent to 3.5 MeV was derived for the best crystal read out with slow signal shaping. However, some low light yield crystals contribute in a dominant way to the total noise for which a value of ~70 MeV was observed.

4. THE MUON/PION CALIBRATION

Muons of 225 GeV/*c* momentum in H4 and pions of 50 GeV/*c* in X_3 aimed at each crystal were used for intercalibration of all segments and also for studying the effect of charged particles passing through the Silicon photodiodes. Figure 3 shows the resulting spectrum for the central front segment, with part of the pions passing through the crystal only and part through crystal and SiPD. The two peaks above the pedestal peak correspond to the Landau distribution of the pion light signal in the crystal (left) and to the convolution of the two Landau distributions due to the crystal light and to the direct effect of particles in the SiPD (right).

As is well known, ionizing particles passing through the depleted zone of a silicon photodiode create electron-hole pairs. A calibration using the ^{57}Co X-rays of 122 and 136 keV energy performed on each SiPD indicated that minimum ionizing particles loose ≈87 keV (peak

value) in 300 μm of silicon. Since 3.6 eV are necessary to create an electron-hole pair in silicon, the signal induced by a muon in a SiPD corresponds to ≈24000 electrons collected. The light peak position for the central front crystal (Fig. 3) is thus determined in number of electrons. The energy deposit in this crystal calculated by Monte-Carlo simulation being 113 MeV, a light yield of ~180 e^-/MeV collected by the photodiode can be deduced.

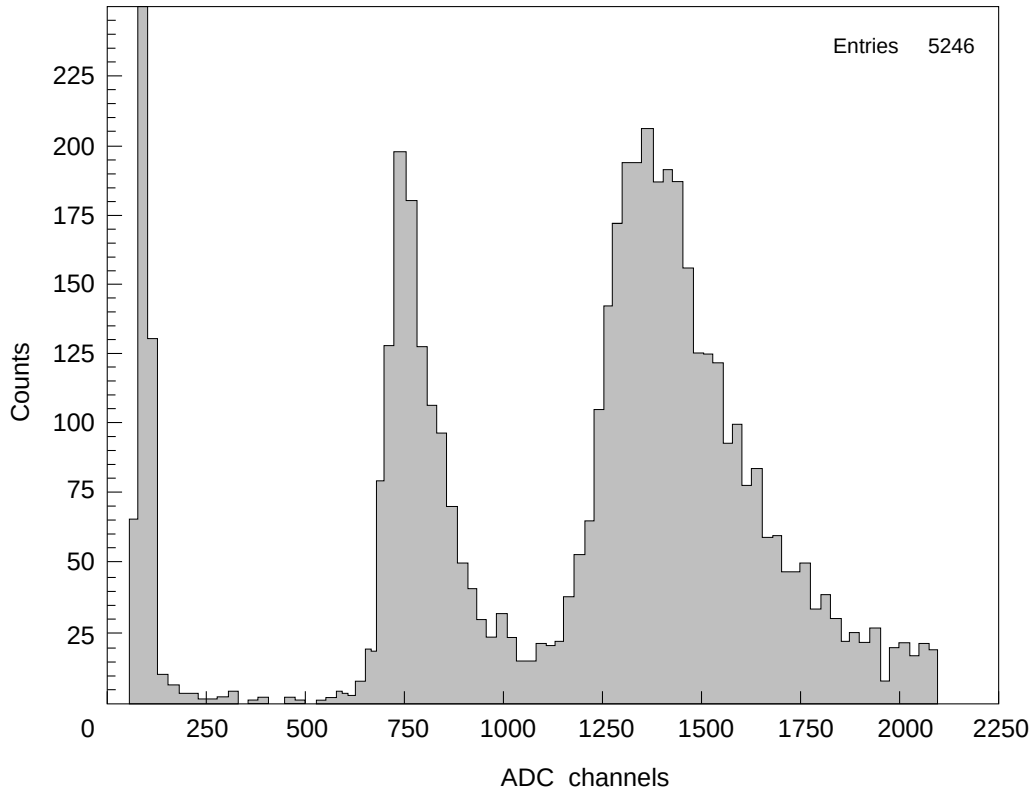

Fig. 3: Pulse height spectrum of pions in the front central crystal. The 3 peaks from left to right correspond to pedestal, to pions traversing the full crystal length and to pions traversing the crystal and the SiPD. Pion interactions are in overflow.

5. ENERGY RESOLUTION

The 50 GeV electron beam was aimed in turn at the center of each tower to obtain the front to back intercalibration factors. For example, the front crystal response in function of the back response for 50 GeV electrons in the central tower is shown in Fig. 4. Fitting linearly the observed correlation yields the front-back intercalibration factor. By comparing the energy measured for 50 GeV electrons in each crystal to the energy deposits predicted by Monte-Carlo, the intercalibration and absolute calibration of each tower were derived. Thus the energy distribution summed over 9 towers (Σ_9), when 50 GeV electrons hit tower 5, was obtained (Fig. 5). Using the observed width at half height or a gaussian fit excluding the tails, one derives a resolution $\sigma/E = 0.7\%$; after deduction of the beam momentum spread, the value $\sigma/E = 0.5\%$ is obtained at 50 GeV.

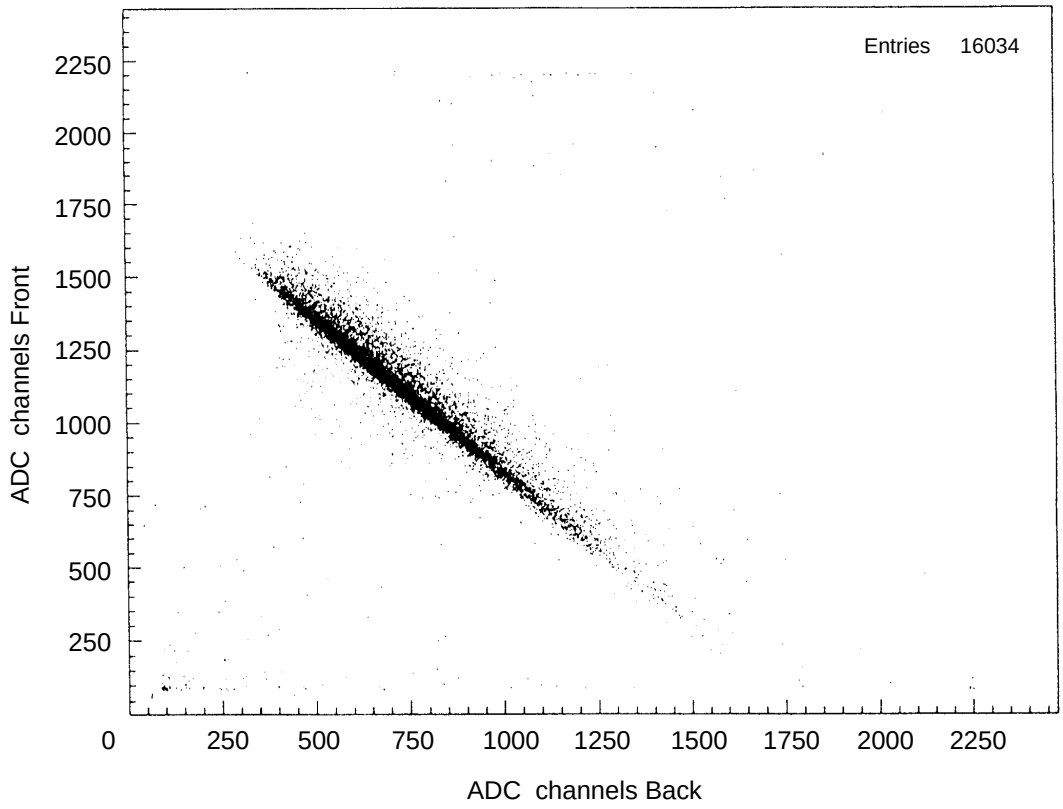

Fig. 4: Correlation between the responses of front and back crystals to 50 GeV electrons in the central tower.

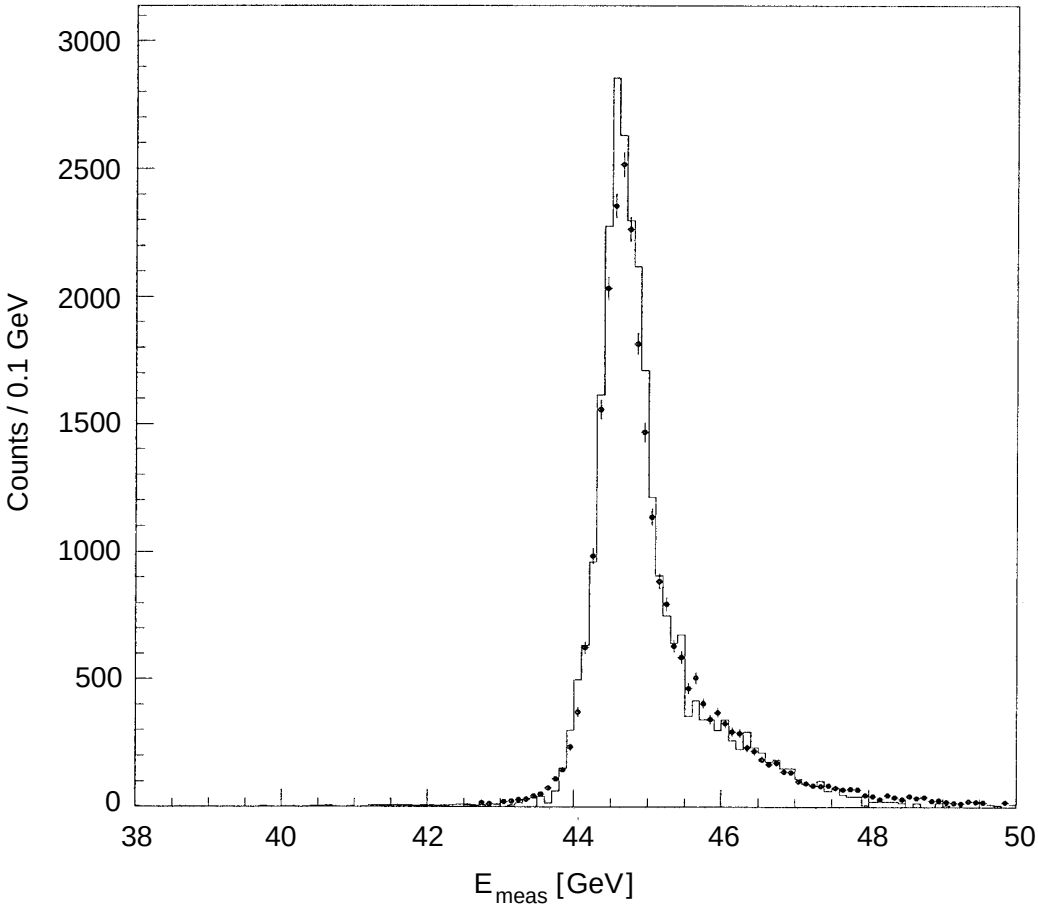

Fig. 5: Energy spectrum (dots) of 50 GeV electrons in Σ_9 towers compared to the Monte-Carlo simulation (histogram) including the nuclear counter effect in the SiPDs.

The high-energy tail observed in the electron spectra can be explained by the interaction of charged particles from the electromagnetic shower in the SiPDs ("nuclear counter effect"). The Monte-Carlo simulation of the spectrum (see Fig. 5) including the SiPD effects shows that peak and tail are rather well simulated. Residual non-uniformities of light collection were found to be negligible.

The nuclear counter effect was studied with the help of auxiliary SiPDs blind to the crystal light, mounted behind the crystal light detecting SiPDs. It can also be seen on single tower spectra for which one or two SiPDs were replaced by photomultipliers (Fig. 6). Charged particles and albedo from the crystal into the front SiPD contribute for more than 50% to the tail, while rear leakage through the back SiPD accounts for the rest. One can see that the nuclear counter effect also slightly increases the energy resolution itself.

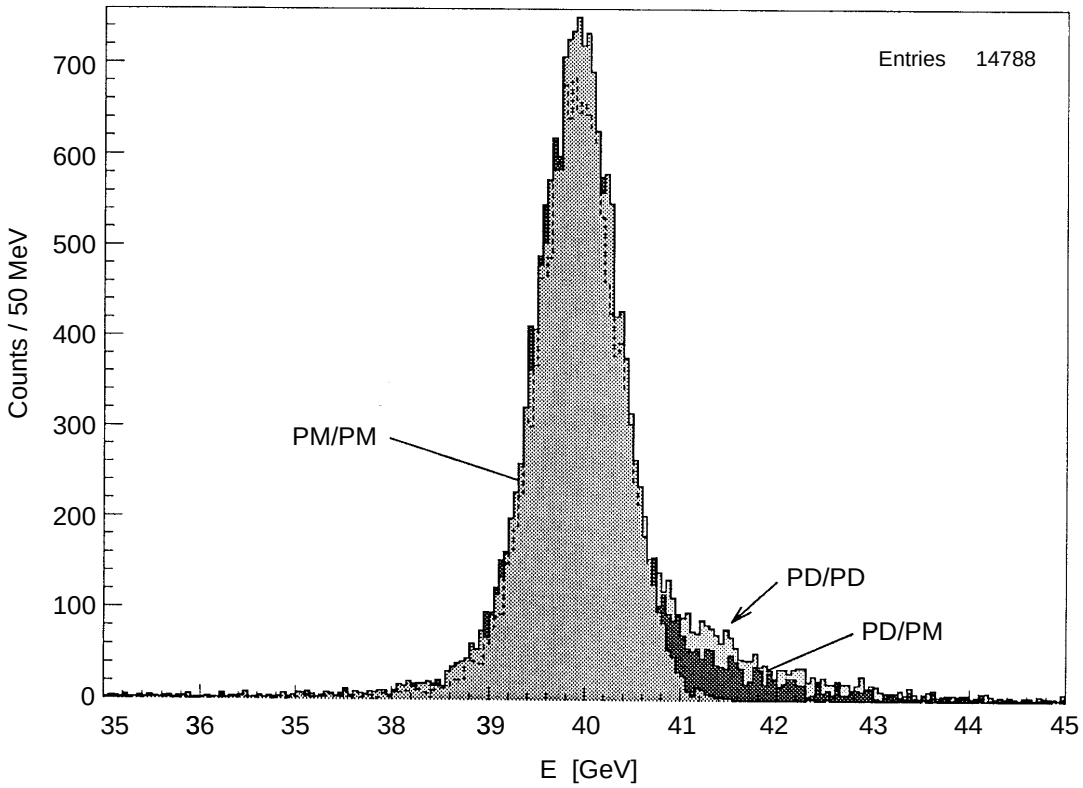

Fig. 6: Energy spectrum of 50 GeV electrons in tower 5 with 2SiPDs (shaded grey), with the back SiPD replaced by a photomultiplier (shaded dark) or with both SiPDs replaced by photomultipliers (dotted line).

Peak positions and energy resolutions (σ/E) were derived at all energies from gaussian fits to the electron spectra within $\pm 1.5\sigma$ from the peak. The peak positions (E_{meas}) relative to the corresponding beam energies (E_{beam}) are plotted in Fig. 7 as a function of beam energy for electrons in Σ_9 towers. The ratios E_{meas}/E_{beam} are normalized to 1 at 80 GeV. Deviations from linearity smaller than $\pm 2\%$ are observed.

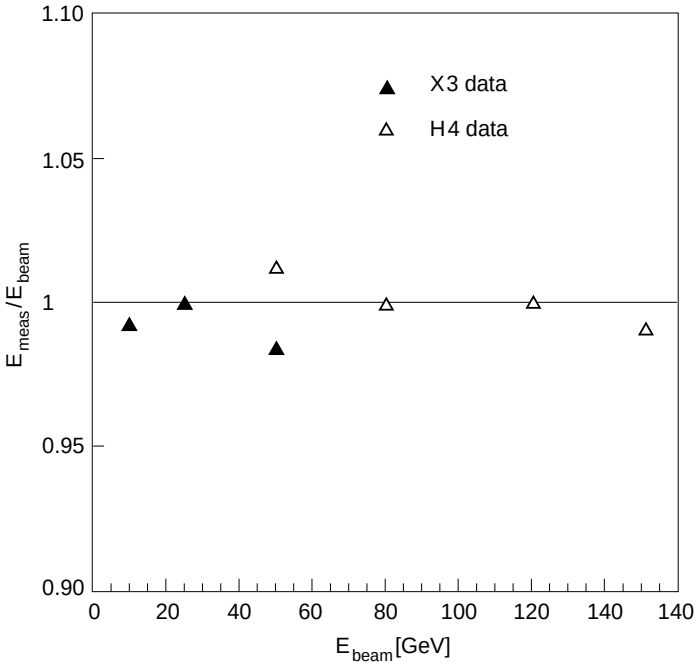

Fig. 7: Variation with beam energy of the ratio E_{meas}/E_{beam} for electrons in Σ_9 towers. The ratios are normalized to the value at 80 GeV.

The corresponding energy resolution values can be seen in Fig. 8. The X3 beam momentum spread of 0.5% was deduced quadratically from the raw resolution, but no correction was applied to the H4 data due to the small intrinsic spread. The measured electronic noise, which in the H4 data contained coherent contributions, was also quadratically subtracted. The agreement of the results with those of a MC simulation including the contributions of direct interactions in front and back SiPDs is very good.

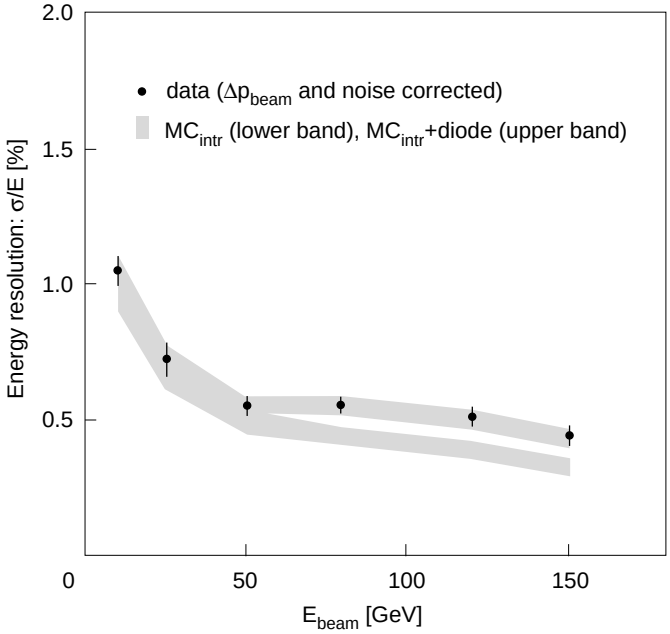

Fig. 8: Energy resolution in Σ_9 towers (black dots) as a function of energy. Beam and noise contributions are substracted. The lower shaded band is the MC prediction for intrinsic resolution. The upper shaded band is a MC which includes nuclear counter effect in front and back SiPDs.

6. RESULTS WITH FAST PREAMPLIFIERS

Various fast preamplifiers were tested on the matrix: two types of current preamplifiers (a discrete bipolar circuit and a CMOS integrated chip) and one charge preamplifier in discrete components. Typically, they have shaping times of about 10–15 ns (i.e. 20–30 ns peaking time).

Results concerning the bipolar circuits which equipped 8 towers of the matrix are presented here. Figure 9 shows a CeF_3 signal for a 50 GeV electron in a single tower with fast current amplification. The signals were integrated in Lecroy 2249W charge integrating ADCs, with a typical gate of 200 ns. The average electronic noise was 2500 e^- for a SiPD of 50 pF capacitance, which corresponds to 12.5 MeV for the crystal with highest light yield. At 50 GeV, a single tower gave a resolution of (1.05 ± 0.02)% to be compared (Fig. 10) to (1.04 ± 0.02)% obtained with slow signal shaping. The global noise for 16 channels was about 300 MeV.

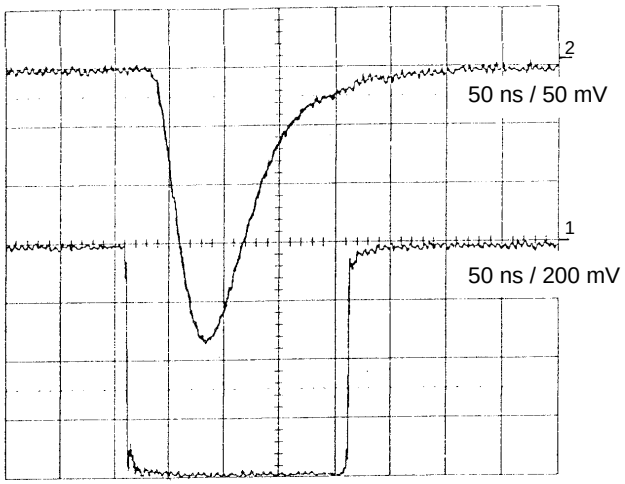

Fig. 9: CeF_3 signal for 50 GeV electrons with a fast current amplifier. The 200ns gate is also shown.

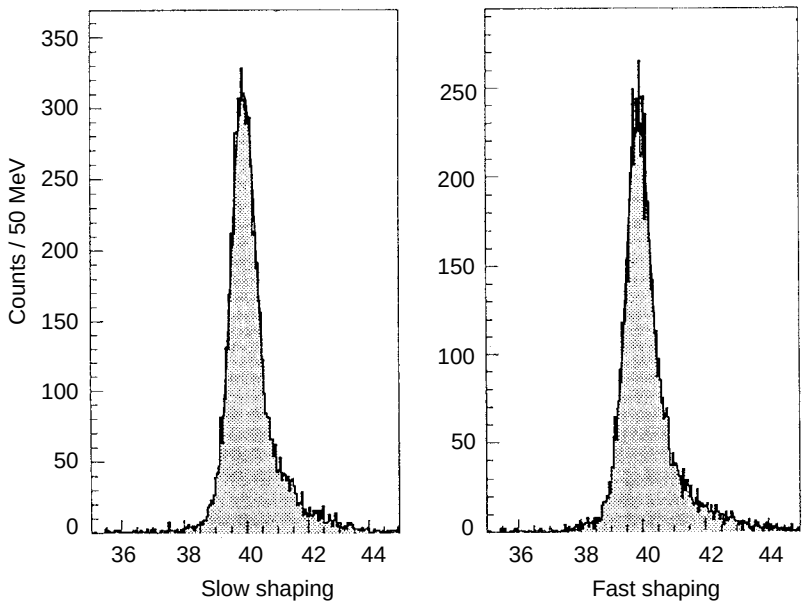

Fig. 10: Energy spectra of 50 GeV electrons in the central tower for short and long shaping times.

These first results show that a resolution compatible with a good calorimeter performance at LHC can be achieved with such fast preamplifiers, provided all CeF_3 crystals have a light yield comparable to our best one. In this case, for 9 towers one would obtain a total noise of:

$$12.5 \times \sqrt{18} \cong 53 \text{ MeV}.$$

7. ELECTRON/HADRON DISCRIMINATION

Besides a precise energy measurement of photons and electrons, an electromagnetic calorimeter at LHC has the important task of identifying electrons in presence of a high hadronic background. Charged pions have a non-negligible probability to simulate electrons by their interactions, mostly through charge exchange. Most of the pions can be rejected by a cut on the total energy deposited in the crystals. In Fig. 11, the Σ_9 spectra measured for pions and electrons of 50 GeV have been superimposed. A cut at 42 GeV yields a 4.7% pion contamination for a 99.5% efficiency for electrons.

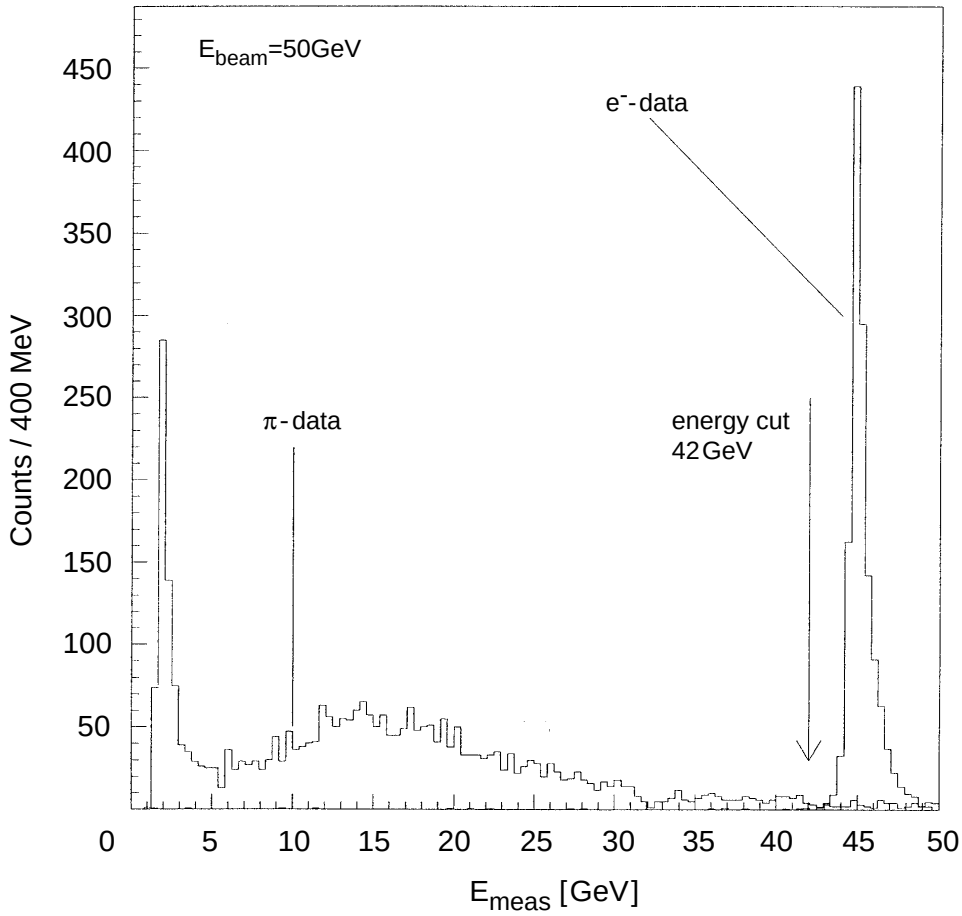

Fig. 11: Superimposed energy spectra of 50 GeV pions and electrons in Σ_9 towers.

Lateral shower extension analysis will bring a further rejection. A cut on the lateral dispersion defined as:

$$D_X = \Sigma E_i x_i^2/\Sigma E_i - (\Sigma E_i x_i/\Sigma E_i)^2$$

can be applied, where E_i is the energy deposit in the i^{th} crystal, centered at a distance x_i along the horizontal axis.

Furthermore, the longitudinal segmentation offers an additional rejection by cutting on the ratio of the energy deposited in the first segments to the total energy: E_{front}/E_{tot} as shown in Fig. 12. The efficiencies obtained for pions and electrons with these cuts are summarized in Table 2. For more details on methods and results, see Ref. [16].

Table 2

Electron/Pion discrimination at 50 GeV in $\Sigma 9$ towers.

Cut on	e efficiency	π contamination
E_{tot} = 42 GeV	99.5%	4.7%
E_{tot} and Dx	99.3%	4.6×10^{-3}
E_{tot} and E_{fro}/E_{tot}	99.4%	1.5×10^{-3}
E_{tot} and E_{fro}/E_{tot} and Dx	99.3%	0.6×10^{-3}

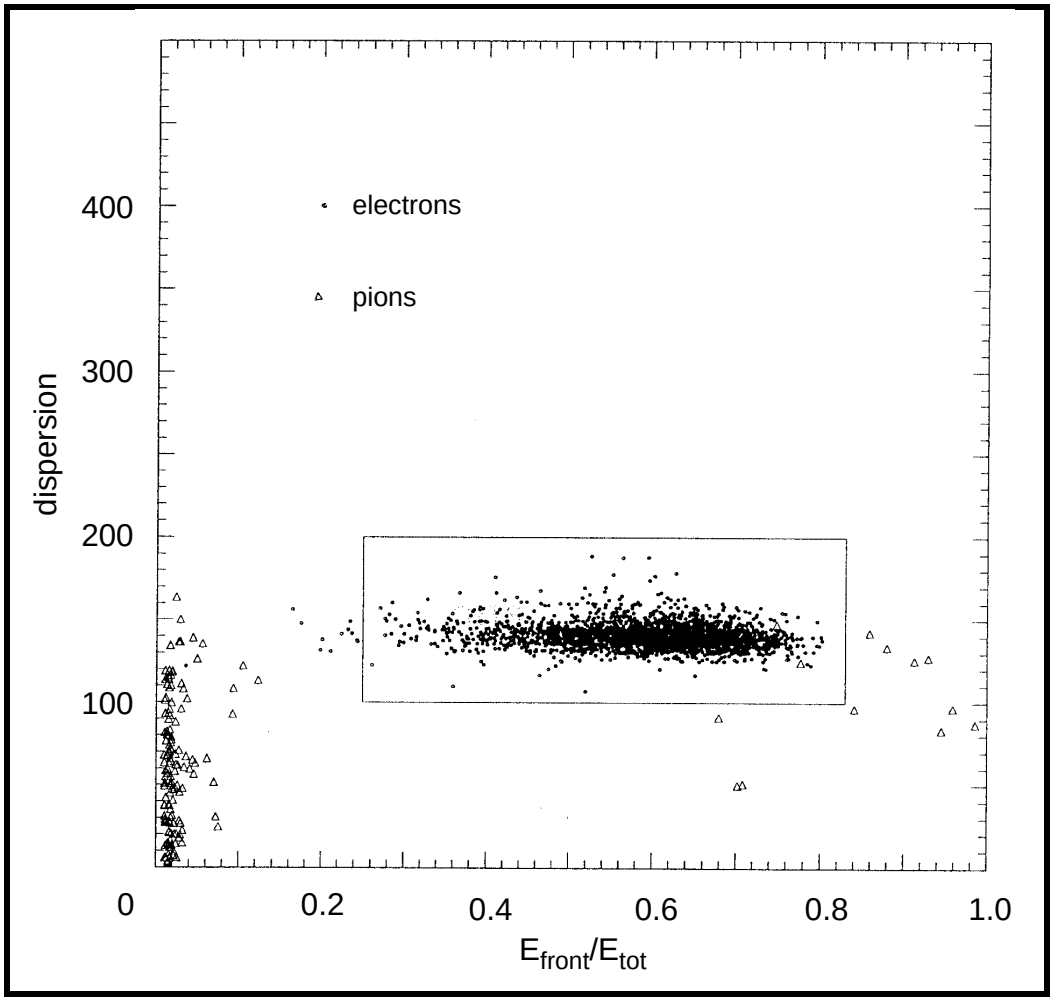

Fig. 12: Scatter plot of the particle dispersion versus the ratio E_{front}/E_{tot}, for pions (dots) and electrons (triangles) superimposed, after the energy cut at 42 GeV was applied. The rectangular cut selecting most of the electrons and 2 pion events is shown.

8. POSITION RESOLUTION AND PHOTON ANGLE

If the granularity of the crystals is chosen to be equal or smaller than the Molière radius,

the lateral spread of the electromagnetic shower over several crystals allows the reconstruction of the impact point of a photon by determination of the barycentre of the energy deposits in the crystals.

Applying classical expressions for the barycentres in the x and y plane, one observes typical S-shape distributions when the barycentre position is plotted in function of the impact point (x_{imp}) known from the beam chambers. A measurement x_{rec} of the impact point is derived from the barycentre position by inverting the fit function to the above distribution. For the difference x_{rec}-x_{imp}, one observes a nearly gaussian distribution, as shown in Fig. 13 for 50 GeV electrons. After unfolding an impact point uncertainty of 0.75 mm, due to the distance from the beam chamber system to the matrix (~3 m), one obtains the resolutions shown in Table 3, which agree with the Monte-Carlo simulation taking into account the geometrical imperfections of the crystals.

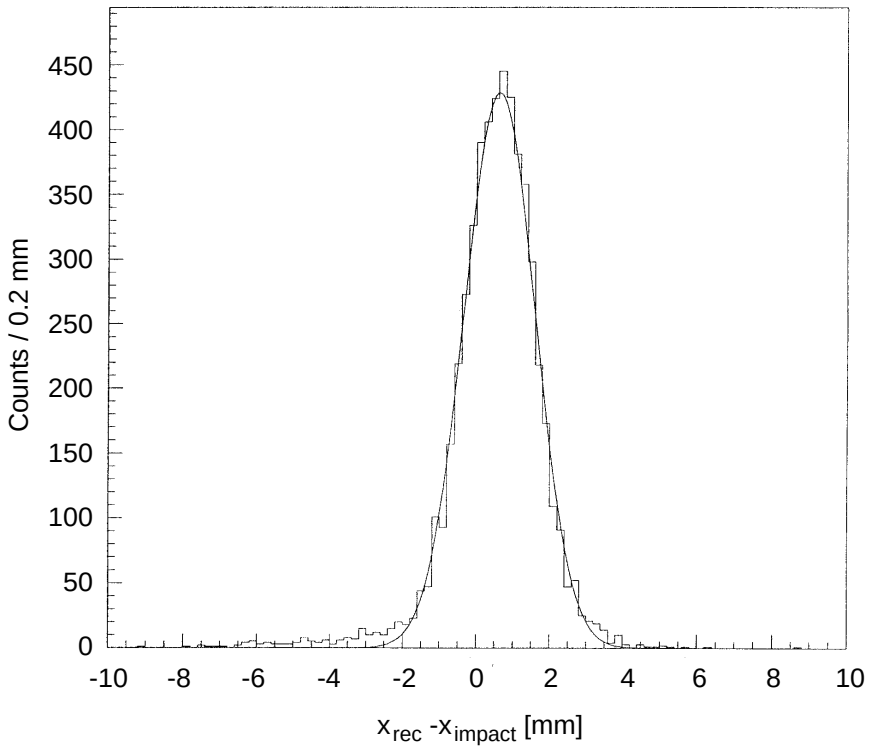

Fig. 13: Distribution of the differences between x-positions reconstructed from the energy depositions in the matrix for 50 GeV electrons and the impact points as measured in the beam chambers.

Table 3

Position resolutions for front, back segments and total towers for 50 GeV electrons.

σ (mm)	Front	Back	Total
x	0.8	1.0	0.67
y	0.85	1.04	0.75

In the case of a collider, the interaction point together with the photon impact point on the

crystal reconstructed from the shower barycentre, allow a precise angular determination of the photon. In particular cases, such as a calorimeter at LHC operating at high luminosity, it may be necessary to reconstruct the photon direction in the calorimeter itself. A longitudinal tower segmentation allows to determine two points of the trajectory, i.e. the two barycentres in 9 front and in 9 back segments for instance.

Simulation of electrons impinging at angles of 1, 2, and 3°, yield the corresponding shifts of back barycentres with respect to front ones. From the relation between lateral shift and angle, a lever arm of ~8.5 cm can be deduced. Using the measured position resolutions listed in Table 3, an angular resolution of 15 mrad for 50 GeV electrons is obtained, corresponding to:

$$\sigma_\theta \cong 100/\sqrt{E} \text{ mrad (E in GeV)}$$

An even better performance could be reached using a finer granularity, shorter front segments and of course a better geometrical accuracy of the crystal arrangement.

9. PHOTODETECTOR TESTS

In complement to the crystal beam tests, two Hamamatsu photosensors were tested in a 3 Tesla magnetic field at CERN: a Si PIN photodiode with preamplifier and a R5189 UV sensitive vacuum phototetrode. Both photodetectors were read out by the same electronics used for the matrix and described in sections 2 and 3. The photodiode was oriented at 45° and 90° with respect to the field and excited either directly with γ-rays from a ^{57}Co source or with the light from a CsI crystal and ^{137}Cs source. The phototetrode was viewing a NaI crystal/^{137}Cs source at field orientations of 30° and 60°.

The photodiode-preamplifier combination showed no detectable sensitivity to the field. The vacuum phototetrode, oriented at 30° and 60° with respect to the magnetic field axis, had its gain significantly affected by the field (see Fig. 14). A decrease of the signal by a factor of ~4 can be observed for 60° orientation. However, for high B values, the gain decrease is slow, so that the phototetrode may be usable at 3 T or even higher.

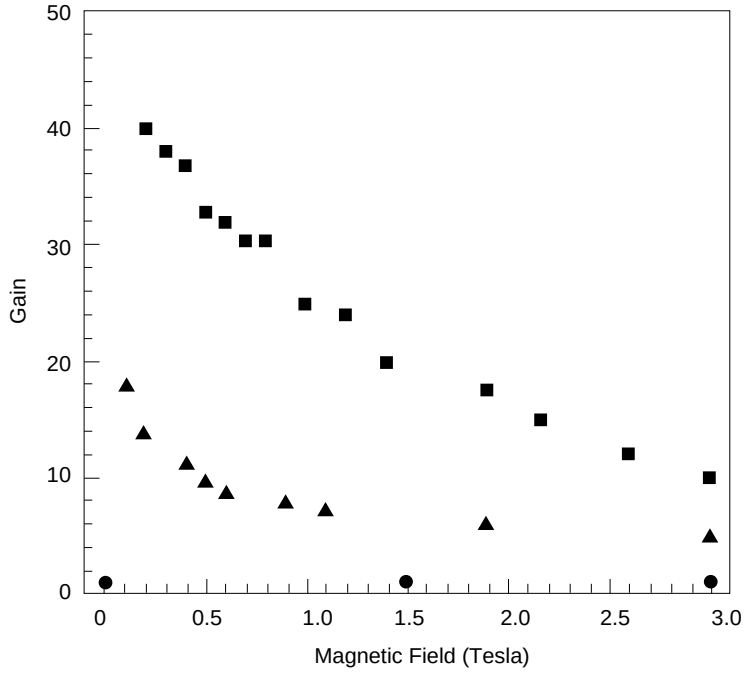

Fig. 14: Magnetic field dependance of the response of a vacuum phototetrode (squares for B at 30°, triangles for B at 60°) and of a Si photodiode (circles).

10. CONCLUSIONS

Our 1994 results represent the first measurement of the performance of a longitudinally segmented CeF_3 crystal matrix, with silicon photodiode readout. In spite of many imperfections in the crystal geometry and large differences in light yield and quality, excellent energy resolutions of the order of 0.5% for electron energies of 50 GeV or more were achieved. From our results, one can conclude that cerium fluoride is presently the best material for homogeneous electromagnetic calorimetry at LHC.

The silicon photodiode readout generates substantial high energy tails in the present conditions. Longer crystals with higher light yields as well as photodiodes optimized in thickness and area should reduce these tails. The use of avalanche photodiodes would suppress the high energy tail entirely.

The fast preamplifiers tested showed a performance adequate for use at LHC.

The longitudinal segmentation, in addition to the large improvement in electron-hadron discrimination, provides photon angle reconstruction to a reasonable accuracy.

CeF_3 crystals, 3×3 cm^2 in cross section and up to 28 cm long, have been produced and smaller high quality crystals are available from several producers. Nevertheless, cost effective mass production of large, consistently high quality crystals remains the key issue for the use of cerium fluoride in large scale detectors at future accelerators.

Acknowledgments

We wish to express our thanks to P. Grafström and N. Doble for their help in operating the X3 and H4 beam lines and to J. Spangaard for his assistance in operating the X3 beam spectrometer. Our thanks also go to the technical staff of the participating institutions for their support.

References

[1] See for instance: G. Altarelli, Summary talk at the ECFA/LHC Workshop, Aachen, October 1990, eds. G. Jarlskog and D. Rein, CERN 90–10 and ECFA 90–133, Vol. I, p. 153.

[2] See for instance: D.Ferrère et al., High resolution crystal calorimetry at LHC, Proc. of the 5th Pisa meeting on advanced detectors, Elba, Italy, May 1991, Nucl. Instrum. Methods, **A315** (1992) 332.

[3] P. Lecoq et al., the Crystal Clear Collaboration, R&D Proposal for the study of new, fast and radiation hard scintillators for calorimetry at LHC, CERN/DRDC P27/91–15, Project RD18.

[4] S. Anderson et al., the Crystal Clear Collaboration, Further results on Cerium Fluoride crystals, Nucl. Instrum. Methods, **A332** (1993) 373.

[5] M. Schneegans, Cerium Fluoride crystals for calorimetry at LHC, Proceedings of the 5th Topical Seminar on Experimental apparatus, San Miniato, May 1993, Nucl. Instrum. Methods, **A344** (1994) 47.

[6] E. Auffray, Ph.D. Thesis, University Paris VI, May 1995.

[7] The Compact Muon Solenoid (CMS), Letter of Intent CERN/LHCC 92–3, LHCC/I1, October 1992.

[8] H. Hillemanns et al., the Crystal Clear Collaboration, First results on large Cerium

Fluoride crystals in a test beam, Proceedings of MRS Spring meeting, April 1994, San Francisco, USA, edited by M.J. Weber et al., Preprint CERN–PPE/94–112, June 1994 and CMS TN/94–235.

[9] U. Dydak, M. Felcini and P. Lecomte, Momentum measurement of the X_3 test beam, CMS technical note CMS–TN/94–252 (1994).

[10] Optical glue "EPOTEC 340", 2 components, n = 1.55.

[11] Millipore, Nº HAWP 293 25 (0.45 μm).

[12] Optical glue "OKEN 6262A".

[13] M. Goyot, Performance of preamplifier-silicon photodiode readout systems associated to large BGO crystal scintillators, Nucl. Instrum. Methods, **A263** (1988) 180.

[14] J.C. Caldero and P. Sahuc, Shaping amplifiers for photodiode readout, Internal Note, IPN Lyon.

[15] 11 bits ADC 811 from ORTEC.

[16] H. Hillemanns, Ph.D. Thesis, University of Aachen, September 1995.